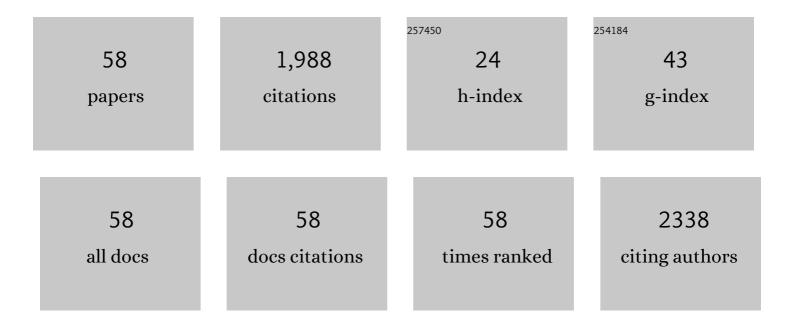
List of Publications by Year in descending order

Source: https://exaly.com/author-pdf/1692424/publications.pdf Version: 2024-02-01



#	Article	IF	CITATIONS
1	Order and Disorder in Layered Double Hydroxides: Lessons Learned from the Green Rust Sulfate─Nikischerite Series. ACS Earth and Space Chemistry, 2022, 6, 322-332.	2.7	3
2	Sulfidation extent of nanoscale zerovalent iron controls selectivity and reactivity with mixed chlorinated hydrocarbons in natural groundwater. Journal of Hazardous Materials, 2022, 431, 128534.	12.4	20
3	Fine-tuning green rustÂâ^'Âbone char composite synthesis for efficient chlorinated ethylene remediation. Chemical Engineering Journal, 2022, 446, 136770.	12.7	1
4	Arsenic removal from natural groundwater using †̃green rust': Solid phase stability and contaminant fate. Journal of Hazardous Materials, 2021, 401, 123327.	12.4	23
5	Fatty Acid Preservation in Modern and Relict Hot-Spring Deposits in Iceland, with Implications for Organics Detection on Mars. Astrobiology, 2021, 21, 60-82.	3.0	8
6	Enhanced sorption of perfluorooctane sulfonate and perfluorooctanoate by hydrotalcites. Environmental Technology and Innovation, 2021, 21, 101231.	6.1	16
7	Siderite nucleation pathways as a function of aqueous solution saturation state at 25°C. Chemical Geology, 2021, 559, 119947.	3.3	7
8	Chlorinated solvent degradation in groundwater by green rust–bone char composite: solute interactions and chlorinated ethylene competition. Environmental Science: Water Research and Technology, 2021, 7, 2043-2053.	2.4	4
9	Arsenic species delay structural ordering during green rust sulfate crystallization from ferrihydrite. Environmental Science: Nano, 2021, 8, 2950-2963.	4.3	6
10	Formation of Formaldehyde and Other Byproducts by TiO2 Photocatalyst Materials. Sustainability, 2021, 13, 4821.	3.2	6
11	A density functional theory study of Fe(II)/Fe(III) distribution in single layer green rust: a cluster approach. Geochemical Transactions, 2021, 22, 3.	0.7	2
12	A novel, direct-push approach for detecting sulfidated nanoparticulate zero valent iron (S-nZVI) in sediments using reactive and non-reactive fluorophores. Journal of Contaminant Hydrology, 2021, 243, 103896.	3.3	1
13	Immobilization of Cr(VI) by sulphate green rust and sulphidized nanoscale zerovalent iron in sand media: batch and column studies. Geochemical Transactions, 2020, 21, 8.	0.7	13
14	Bone Char Mediated Dechlorination of Trichloroethylene by Green Rust. Environmental Science & Technology, 2020, 54, 3643-3652.	10.0	44
15	Effects of metal cation substitution on hexavalent chromium reduction by green rust. Geochemical Transactions, 2020, 21, 2.	0.7	9
16	Direct Visualization of Arsenic Binding on Green Rust Sulfate. Environmental Science & Technology, 2020, 54, 3297-3305.	10.0	26
17	Effects of common groundwater ions on the transformation and reactivity of sulfidized nanoscale zerovalent iron. Chemosphere, 2020, 249, 126137.	8.2	24
18	Hydrotalcite stability during long-term exposure to natural environmental conditions. Environmental Science and Pollution Research, 2020, 27, 23801-23811.	5.3	2

#	Article	IF	CITATIONS
19	Mechanism of Saponite Crystallization from a Rapidly Formed Amorphous Intermediate. Crystal Growth and Design, 2020, 20, 3365-3373.	3.0	16
20	Sorption of chlorinated hydrocarbons from synthetic and natural groundwater by organo-hydrotalcites: Towards their applications as remediation nanoparticles. Chemosphere, 2019, 236, 124369.	8.2	13
21	Hematite Crystallization in the Presence of Organic Matter: Impact on Crystal Properties and Bacterial Dissolution. ACS Earth and Space Chemistry, 2019, 3, 510-518.	2.7	10
22	Adsorption and Reduction of Arsenate during the Fe <sup>2+</sup> -Induced Transformation of Ferrihydrite. ACS Earth and Space Chemistry, 2019, 3, 884-894.	2.7	50
23	The Structure of Sulfidized Zero-Valent Iron by One-Pot Synthesis: Impact on Contaminant Selectivity and Long-Term Performance. Environmental Science & amp; Technology, 2019, 53, 4389-4396.	10.0	99
24	Structural transformation of sulfidized zerovalent iron and its impact on long-term reactivity. Environmental Science: Nano, 2019, 6, 3422-3430.	4.3	31
25	Mechanism of silica–lysozyme composite formation unravelled by in situ fast SAXS. Beilstein Journal of Nanotechnology, 2019, 10, 182-197.	2.8	12
26	Can or cannot green rust reduce chlorinated ethenes?. Energy Procedia, 2018, 146, 173-178.	1.8	16
27	Intercalation of aromatic sulfonates in â€~green rust' via ion exchange. Energy Procedia, 2018, 146, 179-187.	1.8	8
28	Extent of natural attenuation of chlorinated ethenes at a contaminated site in Denmark. Energy Procedia, 2018, 146, 188-193.	1.8	11
29	Microscale Analysis of Fractured Rock Sealed With Microbially Induced CaCO <sub>3</sub> Precipitation: Influence on Hydraulic and Mechanical Performance. Water Resources Research, 2018, 54, 8295-8308.	4.2	42
30	Formation of Silica-Lysozyme Composites Through Co-Precipitation and Adsorption. Frontiers in Materials, 2018, 5, .	2.4	11
31	A Silicate/Glycine Switch To Control the Reactivity of Layered Iron(II)–Iron(III) Hydroxides for Dechlorination of Carbon Tetrachloride. Environmental Science & Technology, 2018, 52, 7876-7883.	10.0	30
32	Immobilization of nanoparticles by occlusion into microbial calcite. Chemical Geology, 2017, 453, 72-79.	3.3	4
33	Impact of Citrate lons on the Nucleation and Growth of Anhydrous CaCO <sub>3</sub> . Crystal Growth and Design, 2017, 17, 5269-5275.	3.0	22
34	How Short-Lived Ikaite Affects Calcite Crystallization. Crystal Growth and Design, 2017, 17, 6224-6230.	3.0	9
35	Prebiotic RNA polymerisation: energetics of nucleotide adsorption and polymerisation on clay mineral surfaces. Chemical Communications, 2017, 53, 12700-12703.	4.1	10
36	Silica and Alumina Nanophases: Natural Processes and Industrial Applications. , 2017, , 293-316.		10

#	Article	IF	CITATIONS
37	Calcite Growth Kinetics: Dependence on Saturation Index, Ca <sup>2+</sup> :CO <sub>3</sub> <sup>2–</sup> Activity Ratio, and Surface Atomic Structure. Crystal Growth and Design, 2016, 16, 3602-3612.	3.0	30
38	Competition between chloride and sulphate during the reformation of calcined hydrotalcite. Applied Clay Science, 2016, 132-133, 650-659.	5.2	23
39	Effect of Aspartic Acid and Glycine on Calcite Growth. Crystal Growth and Design, 2016, 16, 4813-4821.	3.0	36
40	A Microkinetic Model of Calcite Step Growth. Angewandte Chemie - International Edition, 2016, 55, 11086-11090.	13.8	24
41	A Microkinetic Model of Calcite Step Growth. Angewandte Chemie, 2016, 128, 11252-11256.	2.0	18
42	Effect of pH on Amorphous Calcium Carbonate Structure and Transformation. Crystal Growth and Design, 2016, 16, 4500-4508.	3.0	76
43	Citrate Effects on Amorphous Calcium Carbonate (ACC) Structure, Stability, and Crystallization. Advanced Functional Materials, 2015, 25, 3081-3090.	14.9	84
44	Transport of Sporosarcina pasteurii in sandstone and its significance for subsurface engineering technologies. Applied Geochemistry, 2014, 42, 38-44.	3.0	40
45	The Effect of Aspartic Acid and Glycine on Amorphous Calcium Carbonate (ACC) Structure, Stability and Crystallization. Procedia Earth and Planetary Science, 2014, 10, 143-148.	0.6	61
46	In situ and time resolved nucleation and growth of silica nanoparticles forming under simulated geothermal conditions. Geochimica Et Cosmochimica Acta, 2013, 114, 156-168.	3.9	50
47	A Field and Modeling Study of Fractured Rock Permeability Reduction Using Microbially Induced Calcite Precipitation. Environmental Science & amp; Technology, 2013, 47, 13637-13643.	10.0	178
48	Monitoring bacterially induced calcite precipitation in porous media using magnetic resonance imaging and flow measurements. Journal of Contaminant Hydrology, 2013, 152, 35-43.	3.3	26
49	Controls on the rate of ureolysis and the morphology of carbonate precipitated by S. Pasteurii biofilms and limits due to bacterial encapsulation. Ecological Engineering, 2012, 41, 32-40.	3.6	94
50	Microbially mediated plugging of porous media and the impact of differing injection strategies. Ecological Engineering, 2012, 42, 270-278.	3.6	109
51	Comparison of rates of ureolysis between Sporosarcina pasteurii and an indigenous groundwater community under conditions required to precipitate large volumes of calcite. Geochimica Et Cosmochimica Acta, 2011, 75, 3290-3301.	3.9	152
52	Bacterial diversity in five Icelandic geothermal waters: temperature and sinter growth rate effects. Extremophiles, 2011, 15, 473-485.	2.3	64
53	Community Structure of Subsurface Biofilms in the Thermal Sulfidic Caves of Acquasanta Terme, Italy. Applied and Environmental Microbiology, 2010, 76, 5902-5910.	3.1	72
54	Quantification of initial steps of nucleation and growth of silica nanoparticles: An in-situ SAXS and DLS study. Geochimica Et Cosmochimica Acta, 2009, 73, 5377-5393.	3.9	135

#	Article	IF	CITATIONS
55	<i>Inâ€situ</i> grown silica sinters in Icelandic geothermal areas. Geobiology, 2008, 6, 481-502.	2.4	65
56	Controlled biomineralization of magnetite (Fe <sub>3</sub> O <sub>4</sub> ) by <i>Magnetospirillum gryphiswaldense</i> . Mineralogical Magazine, 2008, 72, 333-336.	1.4	28
57	The metagenomics of biosilicification: causes and effects. Mineralogical Magazine, 2008, 72, 221-225.	1.4	2
58	The size and polydispersity of silica nanoparticles under simulated hot spring conditions. Mineralogical Magazine, 2008, 72, 287-290.	1.4	2